Proceedings of the 3rd IASME/WSEAS Int. Conf. on HEAT TRANSFER, THERMAL ENGINEERING AND ENVIRONMENT, Corfu, Greece, August 20-22, 2005 (pp135-140)

Formulation of Four-Tip Optical-fiber Probe for Accurate Characterization of Bubbles

YASUHIRO MIZUNO and TAKAYUKI SAITO[1]
Department of Mechanical Engineering,
Shizuoka University
3-5-1 Johoku, Hamamatsu, Shizuoka 432-8561,
JAPAN.
http://flow.eng.shizuoka.ac.jp/
1: Corresponding author

ABSTRACT: - A reliable four-tip optical-fiber probe (F-TOP) and analysis code have been newly developed for the purpose of characterizing the bubbles in a bubble column. The F-TOP with the code enables high-accuracy measurement of the 3-D motion of the bubbles. In the present paper, the formulations of the F-TOP structure and analysis code are discussed to bring out their best performance. The results measured via the system are compared with those obtained from the visualization of the bubbles using high-speed cameras.

Key-Words: - Multi-phase flow, Four-tip optical fiber probe, Probe signal, Bubble diameter, Bubble velocity, Interfacial phenomena

1 Introduction

Gas-liquid two-phase flows are frequently encountered in a wide range of industrial and scientific fields such as energy technology, material technology, environmental science [1] and technology [2], [3] and so on. The measurement method for bubble characterizations satisfying real time and high accuracy is necessary. Various methods for the bubble characterization have been proposed, however it is very difficult to find a real-time and high-accuracy measurement method applicable to bubble column reactor of high void fraction. In this case, especially, the optical probe method is the most effective. Although much research on the methods has been conducted [4], [5], many difficult problems which have to be solved still remain; e.g., difficulties on pierced chord length, pierced location, bubble orientation and bubble deformation. For the purpose of not only solving the difficulties but also establishing the optical probe method, the Four-Tip Optical-fiber Probe (F-TOP) [6],[7] and analysis code which measure the 3-D motion of bubbles on real time with high accuracy have been newly developed. In this paper, the influences of the existence of the F-TOP on the both motion of the bubbles with various radii and orientations during the contact with it are quantitatively made clear using a high-speed and high-resolution video camera. On the basis of above results, the optimal probe size and analysis code applicable to wide-ranging diameters of bubbles are established.

2 Experiment

2.1 Four-Tip Optical-fiber Probe

The outline of the F-TOP is illustrated in Fig. 1. A plastic optical fiber (Polymethyl- Methacrylate) of 250μm in external diameter; 200μm in core diameter; 25μm in clad thickness was used as the single-tip optical-fiber probe (S-TOP). The beam from a halogen lamp was propagated through each light-source fiber. The optical signal was propagated through each detection fiber, and input into a photo-multiplier. The edge of every probe was cut in an angle of 30 degrees with the fiber axis. Every probe was installed in a stainless capillary of 0.50mm in external diameter.

2.2 Experimental Setup

The probe-bubble contact process as well as the characteristics of the F-TOP signals was investigated using experimental setup shown in Fig. 2. The contact process was visualized using a high-speed and high-resolution video camera (10,000frames/s). In addition, the interface and center-of-gravity motion of free single bubbles (without contact with F-TOP) were also visualized using the same setup and camera. A single bubble was successively form-

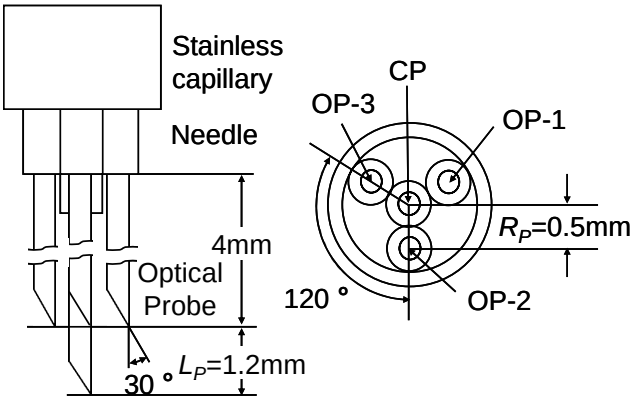

Fig. 1. Structure of F-TOP.

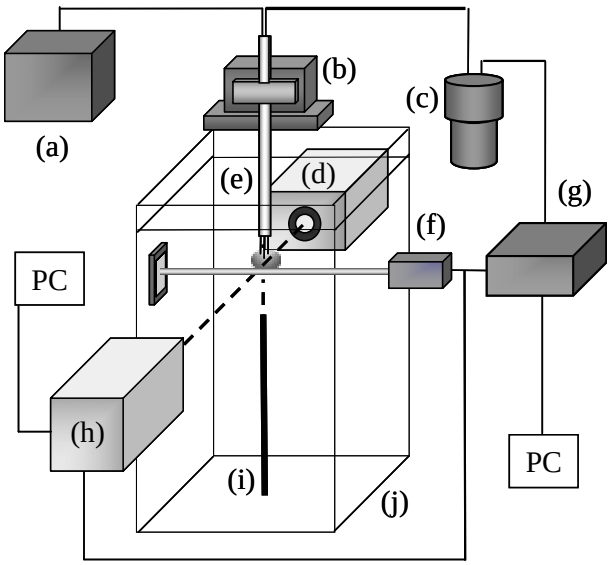

(a) Halogen light, (b) Precision optical stages, (c) Photo multipliers, (d) Halogen light, (e) F-TOP, (f) Laser optic sensor, (g) A/D converter, (h) High-speed video camera, (i) Needle, (j) Acrylic water vessel

Fig. 2. Outline of experimental setup.

ed and released from a needle; in order to examine several kinds of bubble diameter, the needles listed in Table 1 were used. An angle between the F-TOP axis and the direction of the bubble motion, θ_{FB}, was adjusted at 0, 15, 30, 45 and 60 degrees for the purpose of investigating influences of the bubble orientation on the F-TOP signals and the bubble motion (i.e., interface motion and center-of-gravity motion).

Table 1. Internal diameters of needles and the corresponding bubble properties.

Needle	Bubble			
In. Dia. (mm)		Velocity (mm/s)	Major axis (mm)	Minor axis (mm)
0.22	Bubble-1	339.3	3.03	1.31
0.40	Bubble-2	318.7	3.69	1.40
0.66	Bubble-3	289.3	4.19	1.61

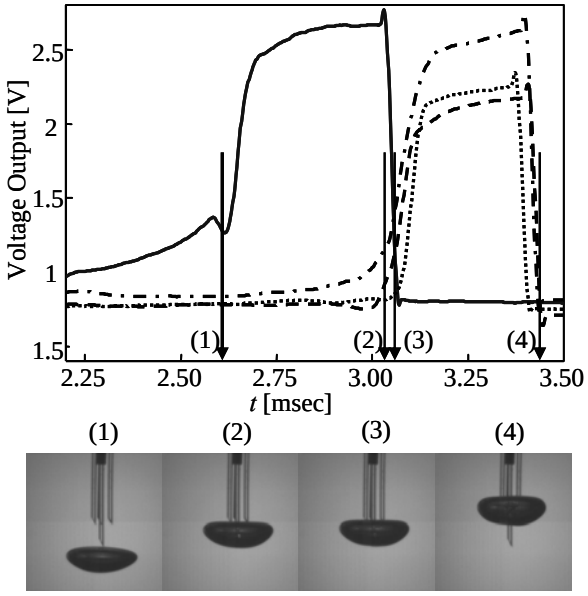

(1) The CP hits the upper bubble interface; (2) The OP-1 hits the frontal bubble interface; (3) The CP hits the bottom interface; (4) Every tip of the F-TOP slips out of the bubble.

Fig. 3. Characteristics of output signals of F-TOP and the corresponding bubble situations.

3 Results and discussion

3.1 Influence of the F-TOP to bubble motion

Typical F-TOP signals and the corresponding bubble images during the contact are shown in Fig. 3. The velocity of the center of gravity, U_{CG}, and the length of minor axis of the bubble, L_{1B}, are obviously influenced by the existence of the F-TOP. The time evolution of velocity change ΔU_{CG} (rate of U_{CG} with the contact to U_{CG} of a non-contact bubble of the same equivalent diameter) during the contact is plotted in Fig. 4 against bubble diameter. The bubble

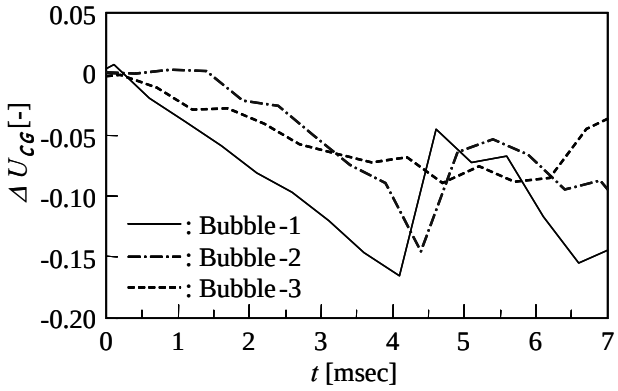

Fig. 4. Time series evolution of ΔU_{CG} during the contact with F-TOP.

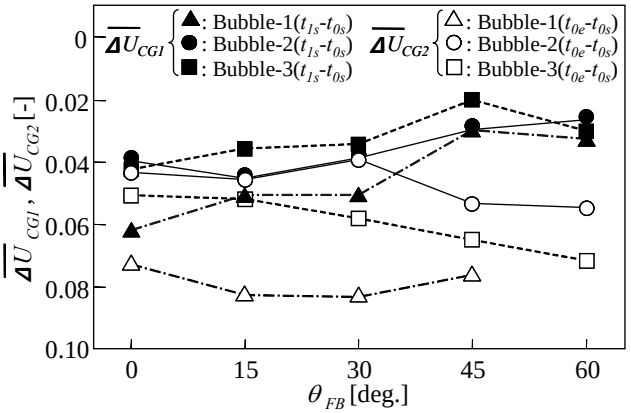

Fig. 5. Relationship between ΔU_{CG} and θ_{FB} against the bubble size.

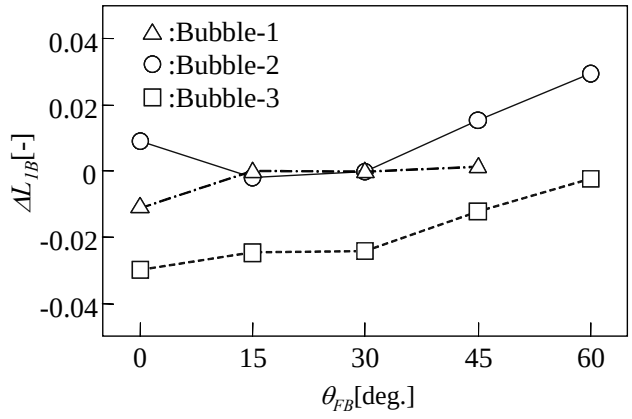

Fig. 6. The relationship between ΔL_{1B} and θ_{FB} against the bubble size.

starts the contact with the CP (: Center probe) at t =0. The bubble velocity decreases immediately after the contact with the CP. The velocity reduction becomes the largest when the CP pierces the bottom interface of the bubble; then the velocity is gradually recovered. The smaller bubble tends to take the larger reduction rate of the velocity.

Figure 5 shows the relationship between $\overline{\Delta U_{CG}}$ (the time average of reduction rate of U_{CG}) and θ_{FB} during the contact by making the bubble diameter into a parameter. The characteristic time is defined as follows: the frontal interface of the bubble touches the CP at t_{cs}, then it touches the OPs (: Outer probes) at t_{1s}, finally the rear interface of the bubble touches the CP at t_{0e}). $\overline{\Delta U_{CG1}}$ is the time average between t_{cs} and t_{1s} (the earlier stage), and $\overline{\Delta U_{CG2}}$ the time average between t_{cs} and t_{0e} (the later stage). The absolute value of $\overline{\Delta U_{CG1}}$ is smaller than that of $\overline{\Delta U_{CG2}}$ in whole cases of bubbles and $\theta_{FB.}$ The velocity in the earlier stage is 2 – 6 % smaller than that of the non-contact bubble. The larger reduction of the bubble velocity occurs against the smaller bubble. From the nature and algorithm of the F-TOP measurement, the influence of the bubble-probe contact in the earlier stage on velocity measurement via F-TOP is considered to be small. The absolute value of $\overline{\Delta U_{CG1}}$ decreases with increase in θ_{FB}. The influence of F-TOP on $\overline{\Delta U_{CG2}}$ tends to be larger for the smaller bubble. This is caused by the fact that the frontal interface of the bubble sooner touches the OPs.

Figure 6 shows the relationship between $\overline{\Delta L_{1B}}$ (time average reduction rate of L_{1B}) and θ_{FB} against the bubble size. L_{1B} of the larger bubble tends to be more intensively influenced by the contact. Absolute value of $\overline{\Delta L_{1B}}$ tends to increase with increase in the equivalent diameter. The influence of the contact on $\overline{\Delta L_{1B}}$ decreases with increase in θ_{FB}.

3.2 Signal processing

The signals from photomultipliers are smoothed via a 25-point moving average method. An example of the typical signals of the F-TOP and the corresponding bubble images are shown in Fig. 3. As the bubble gradually covers the every tip of the F-TOP, the every signal gradually increases with increase in the covered area. On the other hand, when the tip leaves the bubble, the signal falls rapidly. The onset and secession time of the contact are computed using threshold levels as shown in Fig. 7. As indicating the section (A) in Fig. 7, the signal has the section which linearly increases. First, applying the threshold levels to the signal, intersection points (B) and (C) were detected. Second, the point (D) is calculated, which is the intersection point of the straight line of liquid

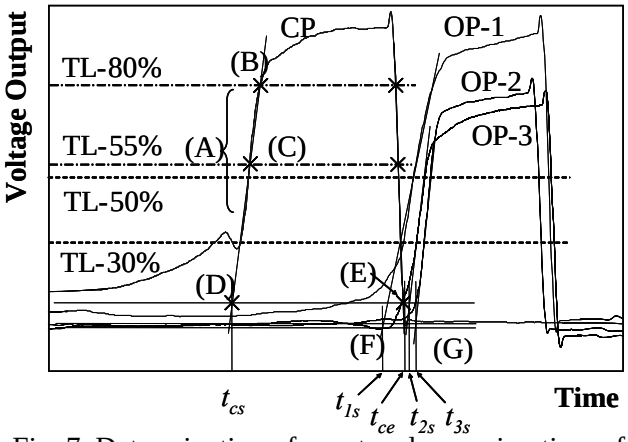

Fig. 7. Determination of onset and secession time of the contact.

phase level and the straight line passing along point (B) and (C). The point (D) is considered to be the onset time of the contact. The secession time was determined as the point (G) employing the similar method. Furthermore, onset time of OP-1, OP-2 and OP-3 are determined by means of the same method.

The bubble velocity was calculated from L_P and the time difference between the onset of the CP and those of the OPs in consideration of the bubble orientation calculated from the onset time differences in OPs. The pierced chord length was calculated from the time bubble passed the CP's tip, t_{1e}-t_{1s}, and the velocity obtained above.

3.3 Probe Calibration

The bubble velocities (F-TOP velocities: U_{CGF}) and minor axes (F-TOP axes: L_{1BF}) obtained using the F-TOP are shown in Fig. 8. When θ_{FB} is 45 or less degrees, the difference between U_{CGF} and the center-of-gravity velocities (visualization velocities: U_{CG}) of the free bubbles measured by high-speed camera were less than 15%. The difference at θ_{FB} = 0 was about 17% in case of the bubble-3 (i.e., the largest bubble), the center probe easily depressed the bubble interface, as a result the period between t_{cs} and t_{1s} was measured longer than that obtained from visualization. The event time, t_{cs}, t_{1s} and t_{ce}, were improved on the basis of the comparison between the events time obtained from F-TOP measurement (F-TOP and original coding) and those obtained from the high-speed visualization. As a whole, the

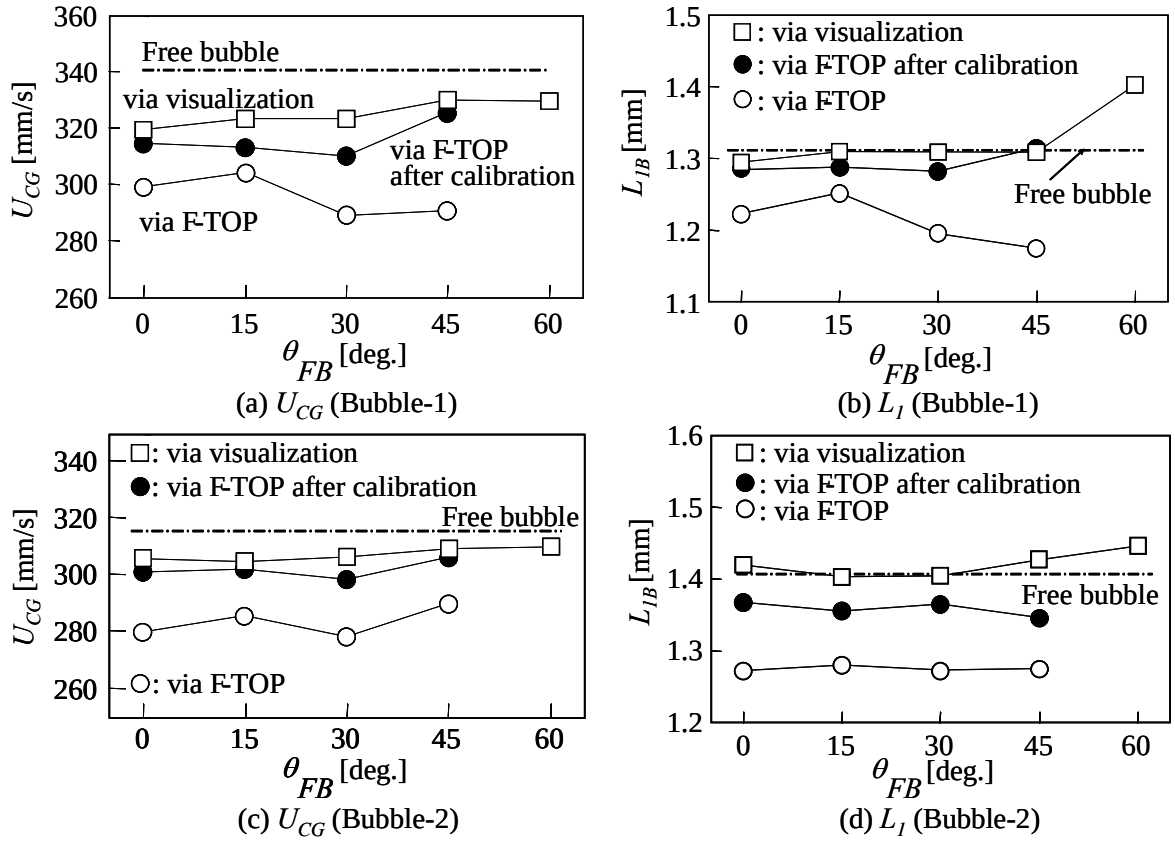

Fig. 8. Comparison of calibration and non-calibration results.

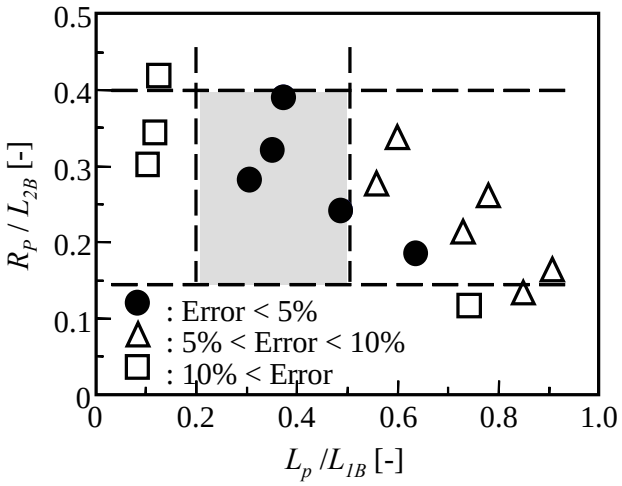

Fig. 9. Measurement accuracy distribution on bubble velocity against F-TOP configuration.

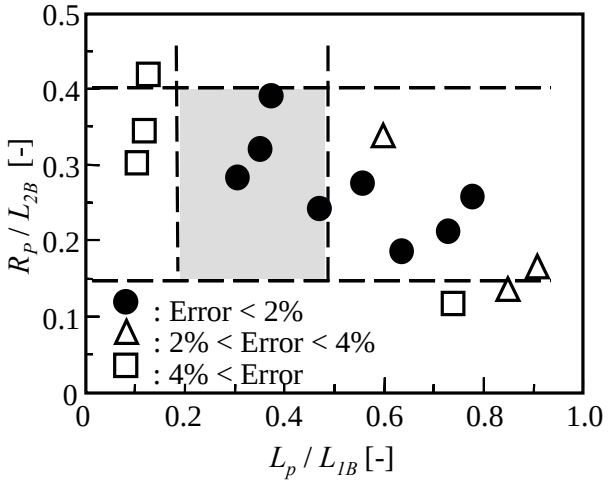

Fig. 10. Measurement accuracy distribution on bubble minor axis against F-TOP configuration.

differences between the calibrated U_{CGF} and U_{CG} were less than 10% at any bubbles except for the bubbles (3) at 0 degree. As a result of calibrating the onset time of the contact from image results, the difference was less than about 5% for any bubbles in $\theta_{FB} \leq 45$ degrees.

3.4 Optimal Design of F-TOP

The relationship between the F-TOP configuration and the measurement accuracy for the bubble velocity and the bubble minor axis is shown in Fig. 9 and Fig. 10, respectively. In the present study, the accuracy is defined as the ratio $|U_{CGF} - U_{CG}|/U_{CG}$ and $|L_{1BF} - L_{1B}|/L_{1B}$. The F-TOP configuration is defined as the ratios of L_P/L_{2B} and R_P/L_{1B}, where L_{2B} is length of the major axis of the bubble. In the case of the bubble velocity, the accuracy is lower when L_P is shorter. However, when L_P is excessively long, the bubble velocity is decreased by the increase of the piercing resistance; as a result the accuracy is declined. On the other, when L_P is excessively short, on set time of the contact becomes uncertain. To determine the optimal L_P is essential for high accuracy measurement via F-TOP. In case of R_P, longer R_P tends to reduce the measurement accuracy. In fact, the longer R_P increases the error, because the outer probes reach the portion of the edge of the bubble. Moreover, conversely, the shorter R_P makes the hollow on the bubble frontal interface. Hence it must reduce the accuracy.

Summarizing the above results and consideration, the optimal L_P and R_P for the high precision measurement should be in the range of 20 to 50% of the average major axis of the two-phase system and in the range of 15 to 40% of the average minor axis of the system.

4 Conclusion

The F-TOP signals and the corresponding process of the bubble-F-TOP contact were simultaneously measured using the high-speed visualization. The influences of the F-TOP on the bubble interface and center-of-gravity motion has been quantitatively clarified. The bubble center-of-gravity velocity during the contact with the F-TOP was reduced; the reduction rate was larger for smaller bubbles. The minor axis of the bubbles was reduced during the contact; the reduction rate was larger for larger bubbles. However, the measurement accuracy was improved by the careful calibration. The optimal probe size for high accuracy was proposed.

ACKNOWLEDGEMENTS

The present study was carried out with the financial support of Scientific Research A No.13355008, Grants-in-Aid for Scientific Research, JSPF (Japan Society for the Promotion of Science). The authors would like to gratefully acknowledge the support of the society.

NOMENCLATURE

CP	center optical probe (see Fig. 1)
L_{1B}	length of minor axis of the bubble
L_{2B}	length of major axis of the bubble
L_{1BF}	bubble minor axis via F-TOP
L_P	vertical length between the tip of center probe and the tip of outer probe (see Fig. 1)
$\overline{\Delta L_{1B}}$	time average of reduction rate of L_{1B}
OP	outer optical probe (see Fig. 1)
R_P	horizontal length between the tip of center probe and the tip of outer probe (see Fig. 1)
t_{js}	onset time of the contact with each optical probe (j = c,1,2,3)
t_{ce}	secession time of the contact with CP
U_{CG}	velocity of the center of gravity of the bubble
U_{CGF}	bubble velocity via F-TOP
ΔU_{CG}	rate of U_{CG} with the contact to U_{CG} of a non-contact bubble of the same equivalent diameter
$\overline{\Delta U_{CG}}$	time average of reduction rate of U_{CG}

Greek symbol

θ_{FB}	angle between the F-TOP axis and the direction of the bubble motion

References:

[1] S. Komori, R. Nagaosa, Y. Murakami, Turbulence Structure and Mass Transfer Across a Sheared Air-Water Interface in Wind-Driven Turbulence, *Journal of Fluid Mechanics*, Vol.249, 1993, pp.161-183.

[2] Saito, T., Kajishima, T. and Nagaosa, R., CO_2 Sequestration at sea by gas-lift system of shallow injection and deep releasing, *Environmental Science & Technology*, Vol.34, 2000, pp.4140-4145.

[3] Saito, T., Kosugi, S., Kajishima, T. and Tsuchiya, K., Characteristics and performance of a deep ocean disposal system for low-purity CO2 gas via a gas lift effect, *Energy & Fuels*, Vol.15, 2001, pp.285-292.

[4] A. Cartellier, Simultaneous void fraction measurement, bubble velocity and size estimation using a single optical probe in gas-liquid two-phase flows, *Review of Scientific Instruments*, Vol.63, 1992, pp.5442-5453.

[5] Clark, N. N. and Turton, R., Chord length distributions related to bubble size distributions in multiphase flows, *International Journal of Multiphase Flow*, Vol.14, No.4, 1988, p.413-424.

[6] R. F. Modde and Satio T., Hydrodynamical similarities between bubble column and bubbly pipe flow, *Journal of Fluid Mechanics,* Vol.437, pp.203-228.

[7] Saito, T., Ishigaki, Y. and Mizuno, Y., Chord length distributions related to bubble size distributions in multiphase flows, *Proceedings of ICMF-2004*, *Fifth International Conference on Multiphase Flow*, Paper No. 113, 2004 in CD-ROM.